The International Journal of Advanced Manufacturing Technology (2021) 113:351–363
https://doi.org/10.1007/s00170-021-06630-5

ORIGINAL ARTICLE

# Alternative materials in moulding elements of hybrid moulds: structural integrity and tribological aspects

Pedro Gonçalves Martinho[1] · António Sérgio Pouzada[2]

Received: 14 March 2020 / Accepted: 11 January 2021 / Published online: 24 January 2021


## Abstract

Hybrid moulds are an increasingly considered alternative for prototype series or short production runs. This type of tools resorts on the use of Rapid Prototyping and Tooling (RPT) to produce the moulding elements (blocks or other inserts). This study was developed using a hybrid injection mould with exchangeable moulding elements that were produced by additive manufacturing (AM), namely vacuum epoxy casting, stereolithography and ProMetal. A full steel tool was also used as a reference. The processing conditions for the polypropylene moulded parts using the hybrid mould were monitored for pressure, temperature and ejection force. The hybrid mould performance was assessed in terms of pressure and temperature evolution during the injection cycle and the AM moulding elements for physical integrity. The data from the polypropylene moulded parts and the moulding inserts are compared with structural and rheological simulations using ANSYS Workbench and MOLDEX 3D. The results show that the hybrid mould performance and the structural integrity of the moulding elements depend on the properties of the materials used. The moulding shrinkage, when resin cores are used, is also affected by the core deformation caused by the injection pressure.

**Keywords** Hybrid mould · Injection moulding · Rapid tooling · Vacuum casting · Polypropylene · Shrinkage · Ejection force · Structural simulation

## 1 Introduction

The use of unconventional materials in moulding blocks of injection moulds has gained interest in the plastic injection moulding industry. This type of moulds, combining a conventional structure and moulding blocks produced in alternative metallic or synthetic materials (e.g. [20]), is known as hybrid moulds. They are an optional solution for small or prototype production series. To produce the moulding blocks, various Rapid Prototyping and Tooling (RPT) techniques are available such as direct rapid tooling as Direct AIM [8] or Selective Laser Sintering or Metallic LOM [10], and indirect processes as Epoxy tooling [3], Spray tooling [18], or 3D KelTool [4]. However, problems have been reported by researchers working with hybrid moulds, namely those associated to the material selection for the moulding blocks [14, 15, 22]; the manufacturing process to produce the moulding blocks [5, 19, 27]; the plastics to be injected; the complexity of the part geometry; and the processing conditions used to produce the part [6, 25].

The application of simulation tools to help the correct mould design and guaranteeing its good performance brings significant improvements. Factors that influence the mould design include the geometric characteristics of the plastic part, the size of the mould, the configuration of the cooling system and its manufacturing technology. The design and optimization of conformal cooling channels in injection moulding tools is regularly published in the literature as, for example, [11]). More recently, a new method for the automatic design of the mould cooling system was proposed on the basis of discrete geometry of the plastic part [16]. Also, it was proposed a method for automatic parting curve generation in injection mould design [9].

✉ Pedro Gonçalves Martinho
pedro.martinho@ipleiria.pt

António Sérgio Pouzada
asp@dep.uminho.pt

[1] CDRSP, School of Technology and Management, Polytechnic of Leiria, Leiria, Portugal

[2] Institute for Polymers and Composites, University of Minho, Guimarães, Portugal

The importance of rapid prototyping, rapid tooling and Computer Aided Design and Engineering (CAD/CAE) technologies were shown in the last decade as tools to rapidly design and produce quality plastics parts [1, 15, 17]. For instance, when using standard CAE tools, only one fixed value for the thermal characteristics can be assigned. The mouldmakers and RT material suppliers use this fixed value not having in mind the temperature dependency of the thermal characteristics and its influence on the CAE simulation analyses. This consideration results in loss of accuracy when designing the hybrid injection mould for thermal performance. Thus, the CAE software tools should include these characteristics for a more accurate simulation and analysis of the thermal behaviour of these tools.

This research work builds up on the knowledge and findings that were previously reported on the effect of using non-metallic moulding blocks on properties and dimensions when designing hybrid moulds [13]. Now, that work was extended to the production of moulding blocks and moulding pins (defined here as moulding elements) using vacuum casting of an epoxy-based composite material, stereolithography (SL) and ProMetal from ExOne GmbH (Germany). The performance of the moulding elements was assessed in terms of functionality, thermal and flow behaviour, structural integrity and moulding reproducibility. These data were compared with those obtained from the mould with standard DIN WNr.1.2311 tool steel moulding elements. The prediction of the performance was made using CAE and structural simulation software.

## 2 Experimental

### 2.1 The moulding part

A part with features implying the use of side cores in the mould was used to replicate typical moulding conditions. Its shape and dimensions are shown in Fig. 1, featuring a lateral 8 mm in diameter circular opening on the left side and a tubular protuberance on the back (Fig. 1a), and a large cavity (Fig. 1b). The inside surface and the tubular detail were moulded using various materials in the respective moulding blocks. The draft angle considered for the side walls of the main body was 3° and the corners were rounded to allow manufacturing the core block also by machining. The nominal thickness is 2 mm and the entire volume is 15.4 $cm^3$.

### 2.2 The hybrid mould

The hybrid mould standard design for the part is shown in Fig. 2. It enables a quick interchangeability of the moulding blocks made from various materials. Details of this hybrid mould were described elsewhere [12].

The cavity (A) and the core (B) moulding blocks can be assembled in the mould structure when the mould is open, without the need to disassemble the tool. This flexible option allows changing the moulding elements without removing the mould from the injection moulding machine. The details of the moulding blocks are shown in Fig. 3.

### 2.3 Moulding block production

The moulding blocks were produced using five materials: (1) tool steel DIN W Nr. 1.2311; (2) epoxy resin composite Biresin L74 (Sika, Stuttgart, Germany) with 60% aluminium powder; (3) epoxy resin composite Biresin L74 (Sika, Stuttgart, Germany) with 15% short steel fibres; (4) WaterShed XC 11120/2 SL resin (DSM Somos, Hoek van Holland, Netherlands); and (5) rapid tooling material ProMetal S4 (ExOne GmbH, Gersthofen, Germany). These materials were used in the moulding blocks with the combinations shown in Table 1.

The use of epoxy composites with fillers, as short steel fibres, with density much higher than the resin requires curing methods that prevent sedimentation until the gel time is achieved. For this purpose, the dynamic process recommended by Sabino Netto [24] was used.

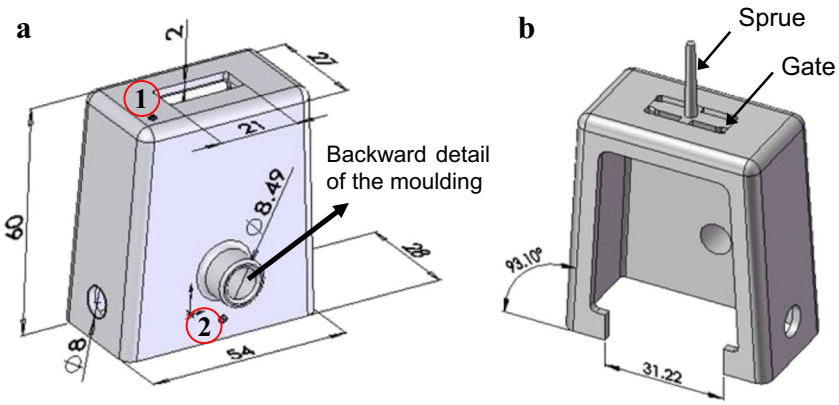


**Fig. 1** Moulding part: **a** main dimensions, **b** part with the runner system

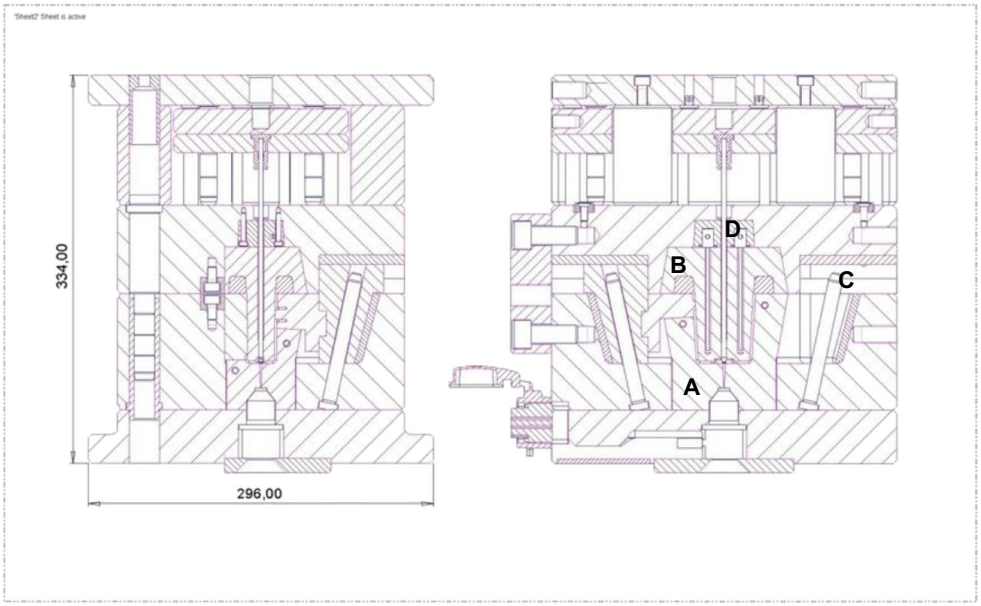


**Fig. 2** Hybrid mould standard design: (**a**) cavity moulding block, (**b**) core moulding block, (**c**) lateral moulding element, (**d**) cooling cassette fitted into the core

The tool steel moulding block (standard) and the non-metallic moulding blocks used in the work are shown in Fig. 4.

The epoxy composite resin cores were produced by vacuum casting in a silicone mould. These cores were made using the actual steel core as a master. The SL resin core block was produced using 3D Systems SLA 3500 equipment, and the ProMetal core block was produced in a R10 ProMetal system (Extrude Hone Corp., Irwin, USA).

The back-hole geometry of the plastic part was defined with a moulding pin that has a draft angle of 0.5° (Fig. 5). These were manufactured using the same five material combinations in Table 1.

The main properties of the moulding elements (blocks and pins) materials are shown in Table 2.

The thermal and mechanical properties of the materials used in the moulding elements (Table 2) were determined with Alambeta conductivity equipment (Sensora, Liberec, Czech Republic), Tritec 2000 dynamic mechanical analyser (Triton, Nottingham, UK) and Zwick Z100 universal testing machine (Zwick, Ulm, Germany). The density of the epoxy-based composite material was determined by the impulsion method. The epoxy Biresin L74 for the composites has a heat deflection temperature of 160 °C.

The epoxy/short steel fibre composite, with low steel carbon fibres with average length of 453 μm and thickness of 45 μm and specific gravity of 7.87 Mg $m^{-3}$ [23], was adopted for the moulding blocks.

The SL moulding elements were produced with an extra thickness of 0.3 mm for the final adjustment of the block to fit into the mould frame.

The aluminium powder particles used in the epoxy/60% aluminium composite are of average size of 50 μm and specific gravity of 2.43 Mg $m^{-3}$.

## 2.4 Mould instrumentation

The hybrid mould was instrumented with integrated pressure and temperature Kistler Type 6190BA sensors (Kistler Instruments, Winterthur, Switzerland) located close to the gate (1) and to the backside detail (2), (cf. Fig. 1).

The pins defining the tubular detail were screwed onto a load cell, specifically designed for this study (Fig. 6).

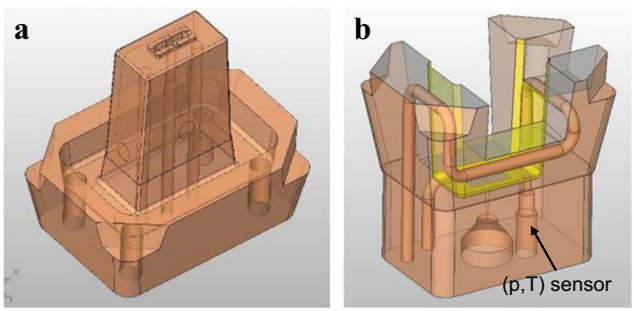


**Fig. 3** Moulding blocks: **a** core, **b** cavity

**Table 1** Combination of the materials for the moulding elements

| Mould code | Material | |
|---|---|---|
| | Core | Cavity |
| R1S | Epoxy Biresin L74/60% aluminium powder | Tool steel |
| R2S | SL resin (DSM Somos 11120/2) | Tool steel |
| R3S | Epoxy Biresin L74/15% short steel fibres | Tool steel |
| PS | ProMetal | Tool steel |
| SS | Tool steel | Tool steel |

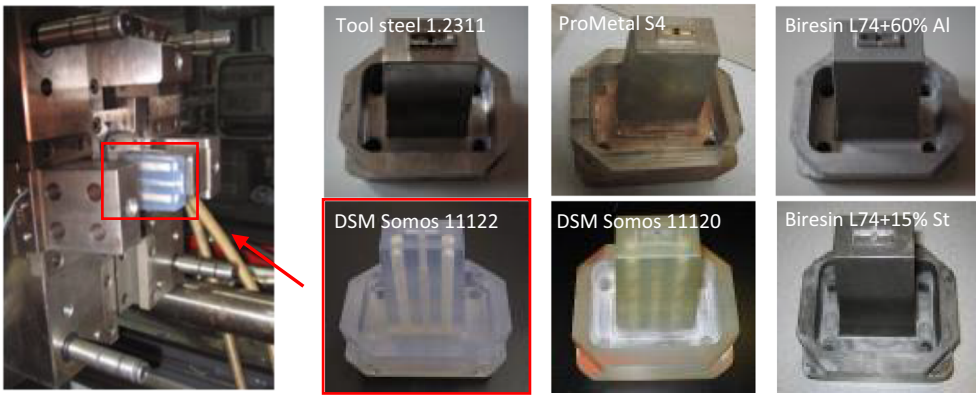


**Fig. 4** Core moulding blocks produced in the various materials

The load cell allows obtaining the force to withdraw the pin from the moulding. These data allow to perform correlations between the moulding element integrity and the ejection force calculation, including its parameters.

### 2.5 Injection moulding

The mouldings were produced in polypropylene homopolymer, PP Homo Domolen 1100N (DOME Polypropylene, Rozenburg, The Netherlands) of MFR 12 g/10 min (230 °C/2.16 kg) using a Ferromatik Milacron K85 injection moulding machine of 850-kN clamping force.

The processing conditions were set according to the materials used on core moulding blocks (Table 3) or according to the materials used on moulding pins (Table 4).

When using the epoxy composite or the SL cores, the processing conditions (pressure and cooling cycle phases) were adjusted to cope with the poorer mechanical properties of these materials. The injection and holding pressures were reduced from the ones that were used for the steel core (by 20% for the epoxy cores and up to 50% for the SL core). The cycle time was increased up to 60 s in all resin core combinations.

For the processing studies with the moulding pin for the tubular feature, it was always used a combination of core and cavity moulding blocks in tool steel, and the processing conditions were adjusted according to the material of the moulding pin, as described in Table 4.

For each injection run, at least 25 mouldings were produced after process stabilization. For each set of new stabilized processing conditions, the first 10 mouldings were rejected.

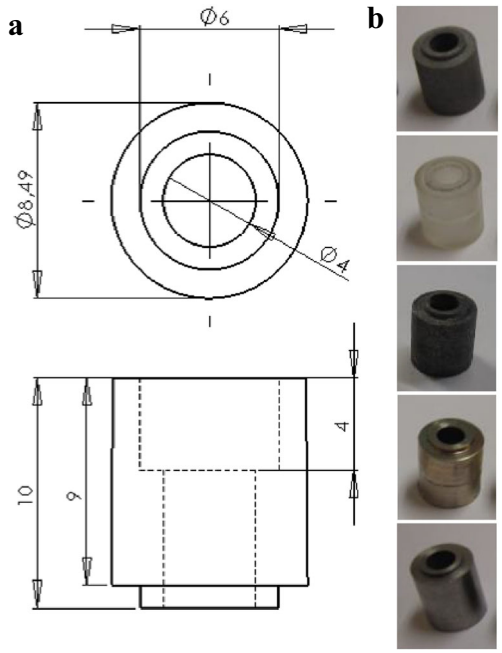


**Fig. 5** Moulding pins: **a** CAD model, **b** produced in various materials

## 3 Results and discussion

### 3.1 Tooling

In injection moulding with hybrid moulds, not only the moulding properties are important but also the moulding elements' integrity, especially when materials with lower resistance are used. With SL resins (R2S combination), the control of the processing conditions was mandatory for extending the lifespan of the moulds. It is recommendable that the process starts with incomplete mouldings produced at lower pressure, and to increase the pressure until complete filling of the impression is achieved. Also, due to the lower thermal conductivity of SL resins, an accurate mould temperature control is required, and longer cooling times are required (Tables 3 and 4).

The failure of the SL core started at the gating region as depicted in Fig. 7.

The complete filling of the parts was only possible with injection pressure of 42 MPa. However, at 28 MPa, vestiges of resin in the mouldings started to appear, as shown in Fig. 8. These occurrences can be associated to the shrinkage and resulting stresses at the gating zone.

The problem was aggravated by the adhesion between the moulded material and the block material. Their Hildebrand

**Table 2** Properties of the materials used in the moulding elements

| | | Tool steel | Epoxy/alum | SL resin | Epoxy/SSF | ProMetal |
|---|---|---|---|---|---|---|
| Properties | Units | (DIN W Nr. 1.2311) | (Biresin L74 +60% Alum) | DSM Somos 11120/2 | (Biresin L74 +15% SSF) | S4 |
| Specific gravity | [Mg $m^{-3}$] | 7.80 | 1.65 | 1.12 | 2.10 | 7.50 |
| Specific heat | [J $kg^{-1}$ $K^{-1}$] | 460 | 1279.19 | 286.26 | _ | 418 |
| Thermal conductivity | [W $m^{-1}$ $K^{-1}$] | 29 | 0.606 | 0.166 | 0.392 | 22.6 |
| Thermal diffusivity | [$m^2$ $s^{-1}$] | _ | $0.286\times10^{-6}$ | $0.519\times10^{-6}$ | _ | $7.2\times10^{-6}$ |
| Thermal expansion coefficient | [$K^{-1}$] | $1.20\times10^{-5}$ | $6.00\times10^{-5}$ | $9.50\times10^{-5}$ | _ | _ |
| Flexural modulus @20 °C | [GPa] | 200 | 5–6 | 2–2.4 | 4.3–4.9 | 147 |

factors of these materials are close (18 $MPa^{1/2}$ for the PP and 22 $MPa^{1/2}$ for the epoxy resin), which implies their adhesion [7]. The low glass temperature of this SL resin (~45 °C) is also an additional problem considering the running temperature of the mould above 60 °C.

The use of epoxy composites, as that in the R1S combination, is more adequate for production. After 300 mouldings, visible defects were not seen in the composite core. The R3S combination with the epoxy/SSF composite in the core shows a similar thermal and mechanical performance. However, when using the R3S combination and especially in sliding zones, it was noticed that small steel particles started to detach from the core moulding block causing seizing in the steel mould surfaces in contact, as shown in Fig. 9. To avoid this problem, it is recommended to use larger gap tolerances in the sliding zones of the mould.

### 3.2 CAE simulation

The Moldex3D (release 9.0) CAE software (CoreTech, Hsinchu, Taiwan) was used for simulating the performance of the hybrid mould. Simulations were based on 1,144,902 tetrahedral elements, from which 177,792 corresponded to the part. The architecture of the cooling system (Fig. 10) was also considered in the simulation.

The prediction of the shrinkage with different moulding materials was performed according to the dimensions shown in Fig. 11.

### 3.3 Comparison of experimental data with simulations

The evolution of pressure and temperature during moulding was monitored for a complete moulding cycle, as shown in Figs. 12 and 13 respectively. Figure 13 shows how the temperature varies at the moulding surface of the core (sensor T2).

As shown in Fig. 12, the peaks reached with the cores in epoxy-based composite resin are lower than those in steel, as expectable from the moulding conditions for these materials. The lower profile in the case of the SL resin is also related with the associated processing conditions.

The data obtained with sensor T2, shown in Fig. 13, highlights the influence of the higher thermal resistance of the moulding blocks with lower thermal conductivity. The lowest temperature curve obtained for the R2S combination is also related with the number of parts injected with this moulding block combination.

The field of temperatures in the pin region as predicted by Moldex3D 9.0 is depicted in Table 5. As mentioned before, in these experiments, only the moulding pin was changed, as the tool steel core and cavity moulding blocks remained.

When low thermal conductivity mould materials are used, the temperature evolution in the first injection cycles changes and it is necessary to know the stabilized 'cruising' mould temperature. The definition of this regime temperature depends on the selected cycle time: rapid cycling leads to higher

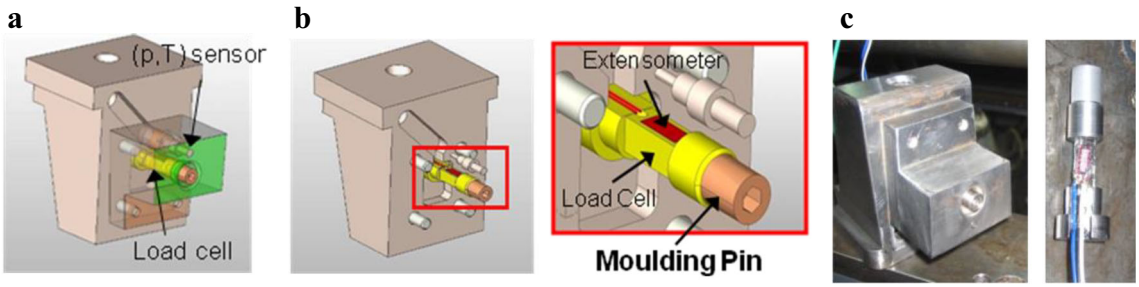


**Fig. 6** Load cell design: **a** hybrid mould side assembly, **b** load cell fitted in the side assembly, **c** view of the load cell

**Table 3** Processing conditions for each mould code combination

| Parameter | Mould code | | |
|---|---|---|---|
| | SS and PS | R1S and R3S | R2S |
| Injection temp [°C] | 230 | 230 | 230 |
| Cooling temp [°C] | 40 | 40 | 40 |
| Injection flow rate [$cm^3\ s^{-1}$] | 37.7 | 37.7 | 37.7 |
| Injection time [s] | 1.3 | 1.3 | 3 |
| Injection pressure [MPa] | 91 | 70 | 42 |
| Holding time [s] | 5 | 10 | 10 |
| Opening, closing and ejection time [s] | 12 | 12 | 12 |
| Holding pressure [MPa] | 70 | 56 | 14 |
| Cooling time [s] | 25 | 35 | 45 |

service temperatures. Figure 14 shows the mould temperature evolution, at the start of each cycle, in the first injection cycles of the R1S hybrid mould. In this case, the mould temperature stabilizes after 12 injections.

From the experimental data in Fig. 14, it is apparent a slight increase of the temperature at the start of each cycle. The simulation also predicts this behaviour. It is also observable a difference of around 5 °C between the experimental and the simulation data. This results from the shrinkage of the polymer creating an air gap between the surfaces of the part and the moulding surface, which may be accounted for in the simulations by applying the so-called thermal contact resistance parameter (TCR). The TCR of the polymer/mould interface is thought to affect the heat transmission coefficient. In the simulations, TCR is considered using the factor $h_{int}$ in the following equations [26]:

$$h_{\text{int}}\left(T_{\text{int}}-T_M^-\right)_{x=-b}=-k\left(\frac{\partial T}{\partial n}\right)_{x=-b} \tag{1}$$

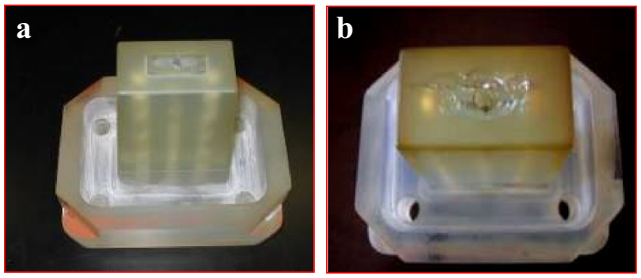


**Fig. 7** Feeding system of the Somos 11120 SL resin core moulding blocks **a** before moulding, and **b** after failure

$$h_{\text{int}}\left(T_{\text{int}}-T_M^+\right)_{x=+b}=-k\left(\frac{\partial T}{\partial n}\right)_{x=+b} \tag{2}$$

where $T_{int}$ is the melt temperature in the interface of the two materials; $T_M^-$ and $T_M^+$ are the moulding zones temperatures, on the cavity side (negative side) and on the core side (positive side), respectively. The indices $-b$ and $+b$ indicate the positive and negative sides of the distance relatively to the centre of the part (equivalent to half of its thickness).

When the thermal conductivity is nil (thermal isolated border), the exchanges between the two materials do not exist. If one assumes an extremely high value, then there would be a perfect thermal contact between the materials and thus the interface temperature is considered identical to the moulding wall temperature. Usually, the default value considered in commercial software is 25,000 W $m^{-2}$ $K^{-1}$.

### 3.4 Shrinkage

In injection moulding with hybrid moulds, the use of soft materials in moulding elements, like epoxy-based composite resins or SL resins, requires a strict control of the processing conditions for the integrity and durability of the inserts. To ensure the mould reliability, it is essential to analyse the polymer shrinkage history, to know the deformation of the moulding components and to assess the mould ejection forces at

**Table 4** Processing conditions according to the moulding pin material

| Parameter | $Pin_1$ (steel) | $Pin_2$ (EP-Al) | $Pin_3$ (SL) | $Pin_4$ (EP-SSF) | $Pin_5$ (ProM) |
|---|---|---|---|---|---|
| Injection temp [°C] | 230 | 230 | 230 | 230 | 230 |
| Cooling temp [°C] | 40 | 40 | 30 | 40 | 40 |
| Injection flow rate [$cm^3\ s^{-1}$] | 37.7 | 37.7 | 37.7 | 37.7 | 37.7 |
| Injection time [s] | 1.3 | 1.3 | 1.3 | 1.3 | 1.3 |
| Injection pressure [MPa] | 91 | 70 | 70 | 70 | 70 |
| Holding time [s] | 5 | 5 | 5 | 5 | 5 |
| Opening, closing and ejection time [s] | 12 | 12 | 12 | 12 | 12 |
| Holding pressure [MPa] | 70 | 56 | 35 | 56 | 70 |
| Cooling time [s] | 25 | 25 | 35 | 25 | 25 |

**Fig. 8** Vestiges of SL resin in the mouldings

critical locations. Moreover, the consideration of the polymer chemical affinity to the moulding surface, expressed by the Hildebrand parameter, and structural analysis are necessary when less stiff materials are used.

Table 6 presents measurements made for the assessment of the shrinkage in the moulding pin zone, between points A and B (Fig. 11(b)).

### 3.5 Mould failure

In this study, after about 20 shots, the failure of the SL inserts occurred as depicted in Fig. 15. The failure resulted from the shrinkage of the moulded material and resulting stresses in this zone.

The problem is worsened by the adhesion between the moulded material and the moulding pin material. These have Hildebrand factors rather close, 18 $MPa^{1/2}$ for the PP and 22 $MPa^{1/2}$ for the epoxy. The low glass temperature of the SL resin (~45 °C) is an additional problem considering the running temperature of the mould. The results show that the use of SL core blocks is not recommended for productions runs over 10–20 parts.

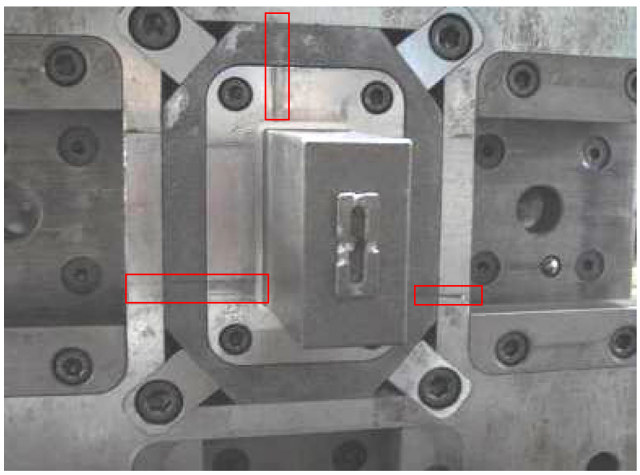

**Fig. 9** Seizing in steel components when epoxy/SSF composites are used in the core

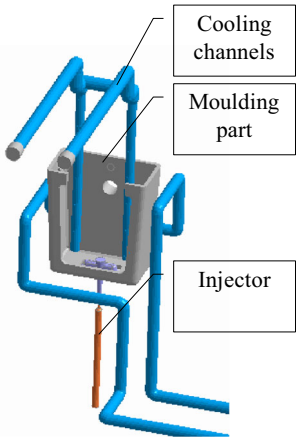


**Fig. 10** Model and cooling architecture used in the Moldex3D 9.0 simulation

### 3.6 Ejection forces

The strain data from the load cell, during the injection cycle, was collected using a Compact DAQ USB data acquisition system (National Instruments, Austin, USA). The linear Eq. (3) obtained in the load cell calibration was:

$$\varepsilon = 8 \times 10^{-6}\, m + 0.0006 \tag{3}$$

where $\varepsilon$ is the corresponding deformation of the cell subjected to a mass $m$, in kilograms.

The corresponding force variation during each injection cycle is shown in Fig. 16.

In Table 7, the experimental data of the recorded ejection forces with the various pin materials are shown as well as the static friction coefficients. These force data are derived from recorded graphs as in Fig. 16, after defining the correct baseline as described in Correia et al. [2], through Eq. (4):

$$F_{\text{eject}} = \left((\varepsilon - 0.0006)/\left(8 \times 10^{-6}\right)\right) \times 9.81 \tag{4}$$

From the shrinkage data and the appropriate static coefficients of friction (coefficients of friction, μ, of pairs of materials in Pouzada et al. [21]), it is possible to estimate ejection forces (Table 7), based on Eq. (5):

$$F_{\text{ejection}} = \mu_e \cdot p_c \cdot A_c \tag{5}$$

where $\mu_e$ is the coefficient of static friction, $p_c$ is the contact pressure acting on the moulding pin and $A_c$ is the pin contact area. To determinate the contact pressure acting on the moulding pin, besides the historical shrinkage of the injection polymer used, it is also important to consider the thermal expansion and the deformation of the materials used on moulding elements. This pressure can be calculated as Eq. (6):

$$p_c = E_{\text{pol}}\left(T_{\text{eject}}\right) \times Sh_i \tag{6}$$

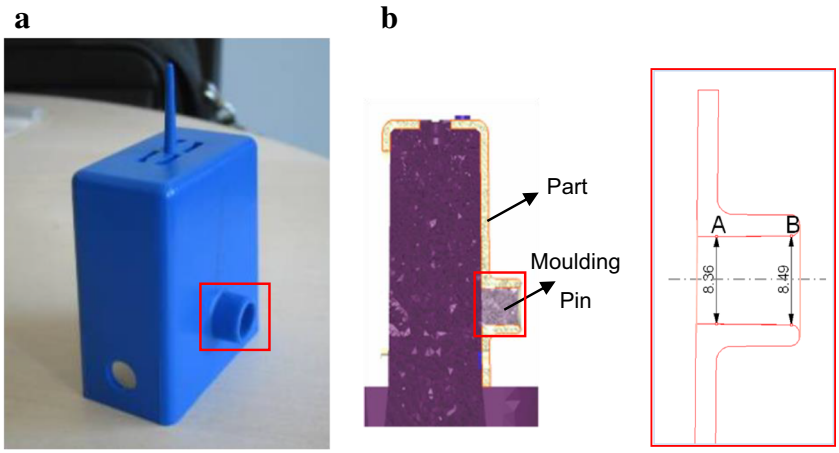


**Fig. 11** Moulding: **a** Back detail, **b** dimensions A and B for shrinkage analysis

where $E_{pol}$ ($T_{eject}$) is the modulus of elasticity at the ejection temperature and $Sh_i$ is the shrinkage of the moulded material.

When metallic materials are used in the mould, $Sh_i$ may be considered depending only on the polymer shrinkage ($Sh_i = f(\delta_{pol})$) because the steel strain is some orders of magnitude lower than the polymer. If lower modulus materials are used in the mould, their strain is of the order of magnitude of the moulded material; therefore, the actual shrinkage of the moulding depends on the polymer itself and also on the moulding element deformation, i.e. $Sh_i = f(\delta_{pol}, \delta_{pressure})$.

The coefficient of thermal expansion of epoxy matrix composites, $\alpha$, is higher than metals. Thus, for the calculation of the contact pressure, it may be necessary to calculate the resulting strain ($\varepsilon_{\Delta T}$) due to the temperature variation from ejection, $T_{eject}$, to ambient, $T_{room}$, Eq. (7):

$$\varepsilon_{\Delta T} = \alpha \times \left(T_{eject} - T_{room}\right) \tag{7}$$

If this strain is significant, i.e. of the same order of magnitude of $Sh_i$, it should be considered in the computation of $F_{eject}$. After these considerations, for the case of a cylindrical pin, Eq. (7) becomes:

$$F_{eject} = \mu_e \times E\left(T_{eject}\right)_{pol} \times \left(Sh_i + \alpha \times \left(T_{eject} - T_{room}\right)\right) \times \pi \times D \times L \tag{8}$$

where $D$ is the diameter of the moulding pin and $L$ the length of the pin in the direction of ejection.

The integrity of moulding pins, at the ejection phase of the injection cycle, was estimated using the pressure data associated to shrinkage of the injected material and the boundary conditions schematized in Fig. 17.

$F_{eject}$ is the ejection force to remove the pin from the back detail of the part, $F_a$ is the friction force and $p_c$ is the contact pressure that can be calculated by Eq. (5).

The ANSYS Workbench 11.0 software was also used to predict the moulding pin structural integrity during the ejection phase. Table 8 shows the equivalent elastic strain and the equivalent stress for the different materials used in moulding pins in the minimum and maximum (or critical) points.

The structural analyses using the software ANSYS Workbench show that the deformations of the pins in Steel and ProMetal are similar as well as the cases of Epoxy/Al and Epoxy/SSF composites. They also show the larger

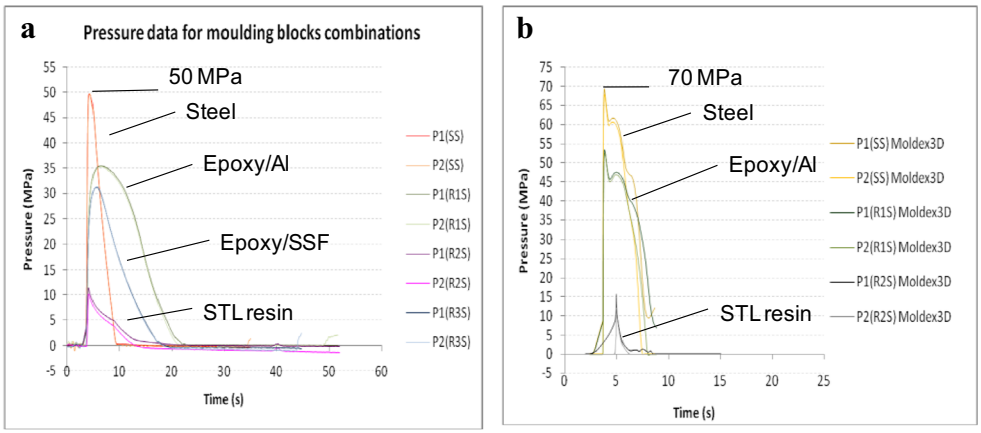


**Fig. 12** Pressure data for the cavity/core combinations: **a** experimental data, **b** prediction in Moldex3D

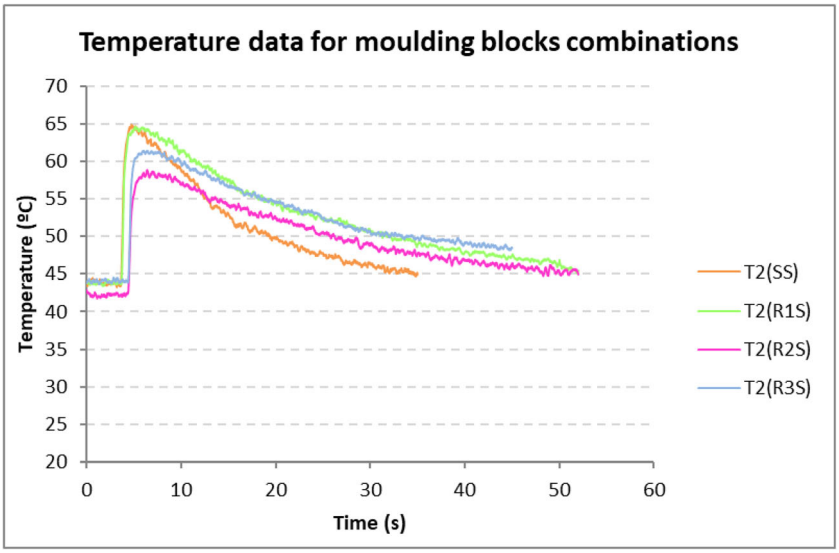


**Fig. 13** Temperature data at the core side

deformation of the soft moulding pin materials, particularly in the case of SL resin where the elastic strain obtained was 2.39% for the equivalent stress (Von-Mises) of 64.32 MPa. As shown before in Fig. 15b, the SL pin failed after 20 shots.

The main mechanical properties of the SL resin are shown in Table 9.

Considering the value of the elasticity modulus of the injected polymer at ejection temperature ($E$ $(T_{\text{eject}})_{\text{pol}}$), 600 MPa (Modulus curves of the PP for 1% strain at 60 °C) and the shrinkage obtained experimentally ($Sh_i$) as 0.0252 (Table 6) in the case of SL resin pin (DSM Somos 11120/2), the obtained contact pressure is 15.12 MPa.

Considering the mechanical properties of the SL resin in Table 9 and the field of stresses obtained in the ANSYS structural analyses of the pins, in as-moulding conditions during the ejection phase, i.e. temperature ≈ 60 °C, ejection force ≈ 690 N and contact pressure caused by the polymer shrinkage ≈ 15.12 MPa, it can be concluded that the failure occurred, most probably, during this phase of the injection cycle.

In this case, the analytical calculation of the equivalent stress showed that the equivalent stress is higher than the interval of values admissible for the tensile strength of the SL resin. For this calculation, it was considered the loading of the pins during the ejection phase and one of the known

**Table 5** Field of temperatures predicted for different moulding pin materials

| Steel DIN W Nr. 1.2311 | ProMetal S4 | Epoxy/Alum | Epoxy/SSF |
|---|---|---|---|
| 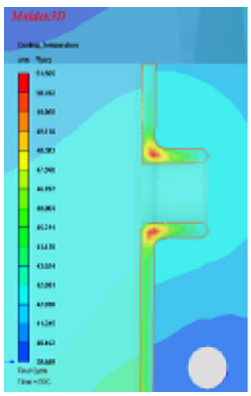 | 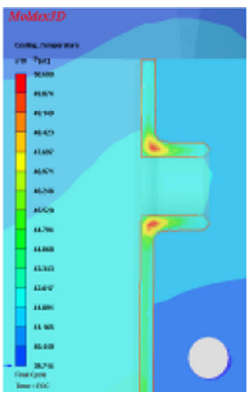 | 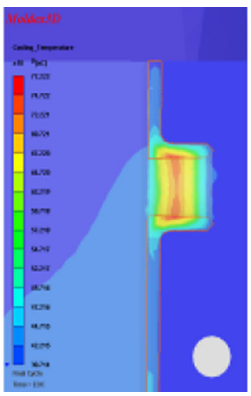 | 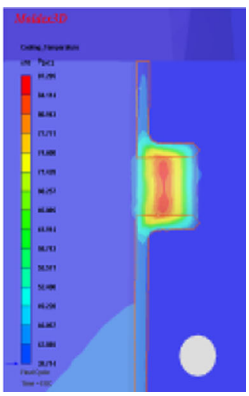 |
| $T_{max}$ = 52ºC | $T_{max}$ = 51ºC | $T_{max}$ = 77ºC | $T_{max}$ = 87ºC |

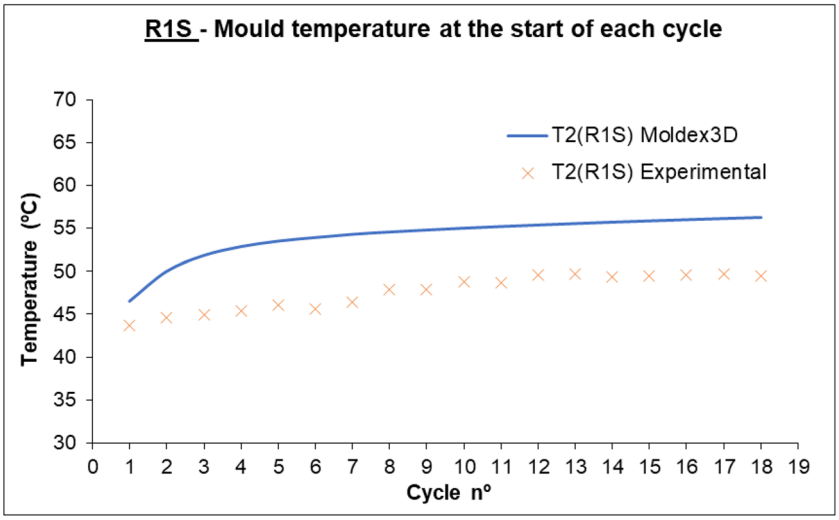


**Fig. 14** Mould temperature evolution during the first moulding cycles using the R1S combination

**Table 6** Dimensions in the moulding pin zone

| Moulding pin material | Shrinkage [%] (measured on the part) | | Shrinkage [%] (Moldex3D 9.1) | | Moldex3D 9.1 relative error [%] | |
|---|---|---|---|---|---|---|
| | A | B | A | B | A | B |
| Steel DIN W Nr. 1.2311 | 2.39 | 1.88 | 2.51 | 1.81 | 5.02 | 3.72 |
| Epoxy/Al | 2.15 | 2.37 | 2.13 | 2.50 | 0.09 | 5.20 |
| DSM Somos 11120/2 | 2.54 | 2.50 | 1.99 | 2.95 | 21.65 | 18.00 |
| Epoxy/SSF | 2.26 | 2.70 | 2.18 | 2.63 | 3.54 | 2.59 |
| ProMetal S4 | 2.40 | 2.02 | 2.48 | 1.87 | 3.23 | 7.4 |
| | | | | Average | 3.85 | |
| | | | | STDV | 2.14 | |

strength materials' criteria (Van Mises or Tresca). Thus, from the ejection force measured by the load cell of 689.70 N for the case of SL resin (Table 6) and the smaller transversal section of $S = 28.34 \times 10^{-6}$ m$^2$ (Fig. 5), the normal stress in the pin is ≈ 24.34 MPa. For the compression stress, it was considered the field of stresses obtained through the ANSYS structural analysis (Fig. 18) with a maximum value of 42.23 MPa, when the pin is only subjected to the contact pressure due the polymer shrinkage.

By using the Mohr's circle for plane stress (Fig. 19) and considering $\sigma_1 = 24.34$ MPa and $\sigma_2 = 42.23$ MPa, the application of the Tresca's criterion ($\sigma_{yield} \geq |\sigma_1 - \sigma_2|$) leads to an equivalent stress of 66.57 MPa that is above the upper limit admissible for the tensile strength, as shown in Table 9.

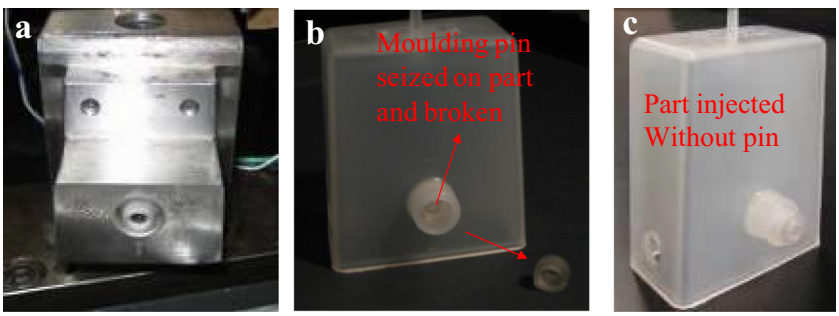


**Fig. 15** Moulding pin in Somos 11120 resin: **a** fitted in the mould; **b** failure on 19th shot; **c** failure on the 20th shot

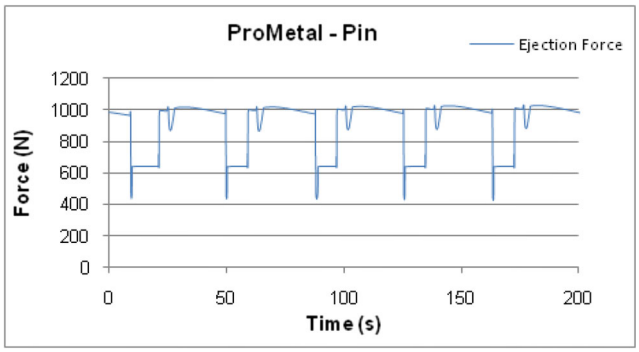


**Fig. 16** Force variation during five consecutive injection cycles

**Table 7** Ejection forces measured in the moulding pin region

| Moulding pin material | Ejection force (N) measured by the load cell | Coefficient of static friction measured | Ejection force (N) estimated |
|---|---|---|---|
| Steel (DIN W Nr. 1.2311) | 415.58 | 0.258 | 434.87 |
| Epoxy/Al | 613.12 | 0.323 | 723.66 |
| DSM Somos 11120/2 | 689.70 | 0.475 | 898.75 |
| Epoxy/SSF | 619.50 | 0.310 | 747.93 |
| ProMetal S4 | 423.79 | 0.257 | 446.50 |

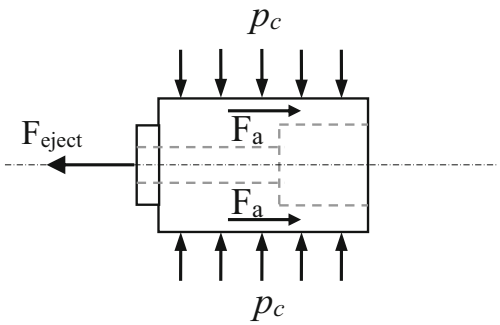


**Fig. 17** Boundary conditions established for the structural analyses in pin inserts

**Table 9** Main mechanical properties of the SL resin

| Mechanical properties | SL resin DSM Somos 11120/2 |
|---|---|
| Tensile strength [MPa] | 47.1–53.6 |
| Elongation at break [%] | 11–20 |
| Elongation at yield [%] | 3.3–3.5 |
| Modulus of elasticity [GPa] | 2.65–2.88 |
| Izod impact notched [J $cm^{-1}$] | 0.2–0.3 |

Source: DSM Somos (New Castle, USA) data sheet

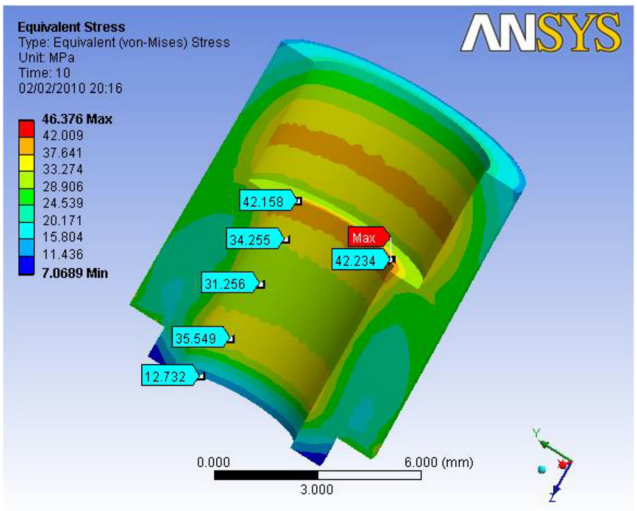


**Fig. 18** Compression stresses on the moulding pin due the polymer shrinkage

## 4 Conclusions

This study on the mechanical and tribological performance of hybrid moulds allows the following conclusions:

i) Hybrid moulds are a suitable solution for producing mouldings of relatively complex shapes.
ii) When softer low thermal conductivity materials are used in the moulding blocks as alternative to steel, their integrity

**Table 8** Equivalent elastic strain and stress of the moulding pins in different materials

| Property vs material | | Tool steel | ProMetal | Epoxy/ SSF | Epoxy/ Al | SLresin |
|---|---|---|---|---|---|---|
| Elastic strain [%] | Min | 0.0029 | 0.0039 | 0.0057 | 0.0051 | 0.0166 |
| | Max | 0.0202 | 0.0389 | 1.3219 | 1.1473 | 2.3890 |
| Stress [MPa] | Min | 3.55 | 3.38 | 0.45 | 0.28 | 0.45 |
| | Max | 56.10 | 58.84 | 60.70 | 63.19 | 64.32 |

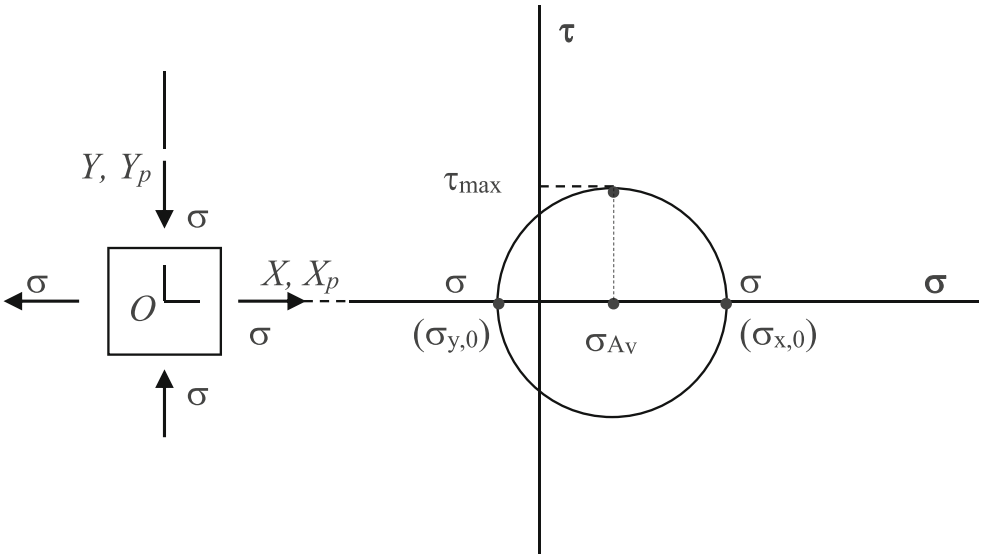


**Fig. 19** Mohr's circle for plane stress for the case of $\tau_{xy} = 0$ and $\sigma_x > \sigma_y$

depends on the processing environment resulting from the imposed cycle time, namely the regime mould temperature.

iii) Computer simulation should be used to predict the thermal behaviour of the mould, considering in the simulation the actual structure of the mould, and the air gap between the moulding and the moulding surface that affects the heat transfer process.

iv) The structural integrity of moulding elements is an issue in hybrid moulds, this being particularly critical when stereolithography elements are used. The structural simulations show that the larger deformation of the soft moulding pin materials implies an increase in the actual shrinkage resulting from the crystallization and thermal shrinkage of the moulded material.

v) The moulding elements made from stereolithography tend to break prematurely and consequently are not recommendable for injection moulds. However, its application can be taken into account for working temperatures below 15 °C above the glass transition temperature of the resin.

vi) The integrity of the non-metallic moulding pins can be estimated from structural analysis using pressure data associated to shrinkage.

**Authors' contributions** Not applicable

**Data availability** Not applicable

## Compliance with ethical standards

**Conflict of interest** The authors declare that they have no conflict of interest.

**Code availability** Not applicable

## References

1. Campbell I, Combrinck J, Beer D, Barnard L (2008) Stereolithography build time estimation based on volumetric calculations. Rapid Prototyp J 14(5):271–279
2. Correia MS, Martinho PG, Pouzada AS (2014) The ejection force effect on the life of hybrid mould inserts produced by additive manufacturing. In: PMI 2014 - International conference on polymers and moulds innovations, Guimaraes, Portugal
3. Curfman WA (1989) Method of making an epoxy mold. General Motors Corporation, Detroit US Patent
4. Drizo A, Pegna J (2006) Environmental impacts of rapid prototyping: an overview of research to date. Rapid Prototyp J 12(2):64–71
5. Freitas A, Soares R, Martinho PG, Pouzada AS (2012) Rapid Prototyping and Tooling in the manufacture of mould elements for large parts. In: PMI 2012 - International conference on polymers and moulds innovations, Gent, Belgium
6. Godec D, Šercer M, Rujnic-Sokele M (2008) Influence of hybrid mould on moulded parts properties. Rapid Prototyp J 14(2):95–101
7. Gonçalves MW, Salmoria GV, Ahrens CH, Pouzada AS (2007) Study of tribological properties of moulds obtained by stereolithography. Virtual Phys Prototyp 2(1):29–36
8. Hopkinson N, Dickens P (2000) A comparison between stereolithography and aluminium injection moulding tooling. Rapid Prototyp J 6(4):253–258
9. Hou B, Huang Z, Zhou H, Li D (2018) A hybrid approach for automatic parting curve generation in injection mold design. Int J Adv Manuf Technol 95:3985–4001
10. Kruth JP, Mercelis P, Vaerenbergh JV, Froyen L, Rombouts M (2003) Advances in selective laser sintering. In: Advanced Research in Virtual and Rapid Prototyping, Leiria/Portugal
11. Marques S, Souza AF, Miranda J, Yadroitsau I (2015) Design of conformal cooling for plastic injection moulding by heat transfer simulation. Polímeros 25(6):564–574
12. Martinho PG, Bártolo PJ, Pouzada AS (2007) Efficient design solutions for hybrid moulds and the widening of the lifecycle of injection moulds. In: PMI 2007 - International conference on polymers and moulds innovations, Gent, Belgium

13. Martinho PG, Bártolo PJ, Pouzada AS (2009) Hybrid moulds: effect of the moulding blocks on the morphology and dimensional properties. Rapid Prototyp J 15(1):71–82
14. Martinho PG, Brito AM, Rodrigues SJ, Pouzada AS (2016) Hybrid moulds: the performance of moulding blocks produced by vacuum casting resins with different fillers. In: PMI 2016 - International conference on polymers and moulds innovations, Gent, Belgium
15. Martinho PG, Cardon L, Neves T, Bártolo PJ, Pouzada AS (2008) A study of the ejection forces on moulding inserts obtained by RPT techniques. In: RPD 2008 - International conference on rapid product development, Oliveira de Azeméis, Portugal
16. Mercado-Colmenero JM, Rubio-Paramio MA, Marquez-Sevillano J d J, Martin-Doñate C (2018) A new method for the automated design of cooling systems in injection molds. Comput Aided Des 104:60–86
17. Nogueira AA, Martinho PG, Brito AM, Pouzada AS (2013) Studies on the mouldability of structural foams in hybrid moulds. Adv Prod Eng Manag 8(2):134–142
18. Palma JM (1999) Metal spray tool repair system. The Boeing company, Seattle Wash.: US Patent
19. Pontes AJ, Queirós M, Bártolo PJ, Pouzada AS (2005) A study on design and performance of hybrid moulds for injection moulding. In: ICIT 2005 - 5th International Conference of Industrial Tools, Bled, Slovenia
20. Pouzada AS (2009) Hybrid moulds: a case of integration of alternative materials and rapid prototyping for tooling. Virtual Phys Prototyp 4(4):195–202
21. Pouzada AS, Ferreira EC, Pontes AJ (2006) Friction properties on moulding thermoplastics. Polym Test 25:1017–1023
22. Ribeiro AR Jr, Hopkinson N, Ahrens CH (2004) Thermal effects on stereolithography tools during injection moulding. Rapid Prototyp J 10(3):176–180
23. Sabino-Netto AC (2008) Desenvolvimento e avaliação de compósito de resina epóxi reforçado com fibras de aço na fabricação de blocos moldantes para moldagem por injeção. Universidade Federal de Santa Catarina, Florianópolis, Tese de Doutorado
24. Sabino-Netto AC, Salmoria GV, Ahrens CH, Pouzada AS (2008) Friction properties of steel fibre reinforced epoxy composites used in moulding blocks of hybrid moulds. Adv Mater Forum IV 587-588:217–221
25. Saurkar S, Malloy RA, McCarthy S (2005) Rapid tooling: a study of different cooling techniques for mold inserts used in the direct aim (ACES injection molding) process. In: Proceedings ANTEC 2005 International Conference, Boston, USA
26. Shojaefard MH, Goudarzi K (2008) The numerical estimation of thermal contact resistance in contacting surfaces. Am J Appl Sci 5(11):1566–1571
27. Silva EC, Sampaio AM, Pontes AJ (2018) Thermal performance of additive manufacturing in hybrid moulds. In: PMI 2018 - International conference on polymers and moulds innovations, Guimarães, Portugal